

Article

Single-Layer Transmitter Array Coil Pattern Evaluation toward a Uniform Vertical Magnetic Field Distribution

Win-Jet Luo ¹, C. Bambang Dwi Kuncoro ^{1,2}, Pratikto ² and Yean-Der Kuan ^{3,*}

¹ Graduate Institute of Precision Manufacturing, National Chin-Yi University of Technology, Taichung 41170, Taiwan; wjluo@ncut.edu.tw (W.-J.L.); kuncoro.bambang@polban.ac.id (C.B.D.K.)

² Electrical and Instrumentation Laboratory, Politeknik Negeri Bandung, Bandung 40012, Indonesia; pratikto@polban.ac.id

³ Department of Refrigeration, Air Conditioning and Energy Engineering, National Chin-Yi University of Technology, Taichung 41170, Taiwan

* Correspondence: ydkuan@ncut.edu.tw; Tel.: +886-4-239-24505 (ext. 8256)

Received: 10 September 2019; Accepted: 28 October 2019; Published: 31 October 2019



Abstract: A uniform magnetic field distribution is a critical aspect in the transmitter array coil design process for achieving a homogenous vertical magnetic field distribution. The free position and orientation features can thus be implemented in the wireless power charging system. This paper presents vertical magnetic field distribution generated by a single-layer circular flat spiral air core transmitter array coil model analysis and evaluation using a numerical analysis method. This method is developed based on the off-symmetry axis magnetic field distribution due to a circular current loop derived from the Biot-Savart law. The proposed evaluation criteria are used to obtain the vertical magnetic field distribution characteristic of the evaluated array coil model. The vertical magnetic field distribution of several circular flat spiral air core coils, in both single and array coil models with different coil geometries were investigated to obtain the relation between the coil parameters and the distance between the adjoining coil centers to generate uniform vertical magnetic field distribution. A case study was also conducted to analyze and evaluate several array coil model patterns (1 × 2 array coil, 1 × 3 array coil, 2 × 2 array coil, 2 × 3 array coil) to meet uniform vertical magnetic field distribution. The array coil model is composed of an identical single circular flat spiral air-core coil. Every single coil has inner coil diameter (D_i), outer coil diameter (D_o), wire diameter (W), pitch (P) and a number of turns (N) at 25 mm, 47.8 mm, 0.643 mm, 0.03 mm, 17 respectively. The study and evaluation of several array coil pattern models show that the distance between the adjoining coil centers should be defined close to the half of coil outer diameter ($1/2D_o$) to generate close to uniform vertical magnetic field distribution. The vertical magnetic field distribution average and magnetic field effective transmitting areas array coil model with the given coil parameters changing as the effect in variation in distances between the adjoining coil centers.

Keywords: coil; array; magnetic field; uniform; wireless power

1. Introduction

Wireless power transmission (WPT) systems have been become fascinating re-emerging technology in recent years. By increasing the overall system efficiency, this technology is appealing to various applications because of its convenience and better user experience. Among those applications, coil geometry and structure study in portable electronic charger applications is attractive to achieve uniform magnetic field distribution.

The study of magnetic fields generated by coils is important in various new coil structures and several widespread applications in portable electronic equipment [1–4], car battery charging [5], biomedical engineering [6], and electromagnetic interference [7]. The coil geometry and structure analysis should therefore be considered as the first step in wireless power transmission system design.

Circular flat spiral coil geometry has been widely employed in WPT studies compared with other coil geometries. However, coil geometry analysis and design is still difficult in practice due to the complex magnetic coupling between the coils.

It is necessary to use computational electromagnetic tools to simplify coil structure analysis and design. Studies on the coil structure for magnetic field generation have been published in recent years by various authors [8–16]. In [8] the authors presented magnetic field planar spiral coil calculations at a given point using vector magnetic potential. Unfortunately, they did not describe the planar spiral coil magnetic field distribution calculation method. They focused on magnetic forces calculation between the planar spiral coil. The spiral shaped coil magnetic field was calculated and measured in [9]. They used the Biot-Savart law to obtain the magnetic field of a given point on the coil loop the axis at a given distance from the coil center. Authors in [10] computed the magnetic field intensity (H) along the axis of a concentric current-carrying loop. In the case of N concentric loops, the sum of a single-turn H-field with different radii was calculated to obtain N concentric loop H-field. Homogeneous coupling between different diameter coils is achieved using the turn distribution method as described for a single coil in [11]. In this method, the current density distribution which generates a homogenous magnetic field is calculated for a single coil. A discrete approach is then used to divide the current trace associated with the magnetic field at different positions. In [12], the authors improved the algorithm presented in [11] which restricted the number of traces. However, they used the same method to calculate the magnetic field distribution. The author in [13] presented spatial magnetic flux density distribution estimation generated by a coil formed by N independent coils. They calculated the magnetic field using the Biot-Savart law by simplifying the current path follows a close trajectory formed by line segments. However, this calculation is not valid for an arbitrary point on any coil position planes. In [14], the authors presented magnetic field distribution calculation on planar concentric coils using the formula derived from the vertical magnetic field generated by a circular current loop in a closed loop. This formula calculated only the magnetic field along the coil center axis and it is not valid for arbitrary points. The authors in [15] used a vector potential to compute the magnetic field at an arbitrary point of a spiral coil in a cylindrical coordinate system. In [16], the authors calculated magnetic flux density using the Biot-Savart law, but they did not describe in detail the magnetic field distribution computation. They focused on the detection of lateral misalignments in an inductive power transfer. However, these studies focused on the magnetic field analysis and evaluation of a single circular coil structure along the coil center axis or at any point in the xz or yz planes in Cartesian coordinates. They did not present an array coil model magnetic field calculation at arbitrary points to obtain the magnetic field distribution. While another study in [17] was concerned with a multilayer planar platform, the authors presented a finite-element (FE) simulation study to simulate the magnetic field distribution of multilayer (three-layer hexagonal) PCB winding arrays using Ansoft Maxwell 3D FE software.

This paper presents a magnetic field distribution analysis and evaluation generated by a single-layer transmitter array coil model using a numerical method. The analysis and evaluation method are developed based on off-symmetry axis magnetic field distribution due to a circular current loop derived from the Biot-Savart law. The proposed evaluation criteria are then applied to obtain the vertical magnetic field distribution characteristic in both single and array coil with different coil geometries. The analysis objective is to obtain a uniform magnetic field vertical distribution toward free-positioning and orientating features in wireless power charger application. Thus, the general magnetic field distribution characteristic of the evaluated array coil is adopted as the coil array design guide in the practical applications. This analysis and evaluation method also applied to several array coil model

patterns (1×2 array coil, 1×3 array coil, 2×2 array coil, 2×3 array coil) in the case study for evaluating their magnetic field distribution to achieve uniform magnetic field vertical distribution.

2. Materials and Methods

2.1. Biot-Savart Law

The magnetic field source comes from currents which arise because of the charge motion. Figure 1 shows that when current flows through a wire, a magnetic field will exist around the wire. The total number of magnetic field ($d\mathbf{B}$) contributions from all small wire segments ($d\mathbf{l}$) at any point (Q) around the wire is the magnetic field at point Q [18].

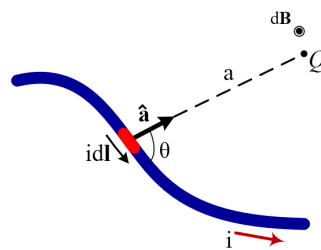


Figure 1. Magnetic field $d\mathbf{B}$ at point Q due to a current-carrying element $id\mathbf{l}$.

The Biot-Savart law expresses the magnetic field contribution as follows:

$$d\mathbf{B} = \frac{\mu_0}{4\pi} \frac{id\mathbf{l} \times \hat{\mathbf{a}}}{a^2} \quad (1)$$

where $d\mathbf{B}$ is the magnetic field contribution in Tesla (T), $id\mathbf{l}$ is the segment current in Ampere (A), a is the distance from the current source to the field point Q in meter (m), $\hat{\mathbf{a}}$ the corresponding unit vector and μ_0 is the permeability of free space:

$$\mu_0 = 4\pi \times 10^{-7} \text{ T}\cdot\text{m/A} \quad (2)$$

The total magnetic field contribution at the point Q is a vector integral of the magnetic field contribution ($d\mathbf{B}$) as follows:

$$\mathbf{B} = \oint d\mathbf{B} = \frac{\mu_0 i}{4\pi} \oint \frac{d\mathbf{l} \times \hat{\mathbf{a}}}{a^2} \quad (3)$$

2.2. The Off-Symmetrical Axis Magnetic Field Formulation due to a Circular Current Loop

The off-symmetrical axis magnetic field due to a circular current loop is illustrated in Figure 2.

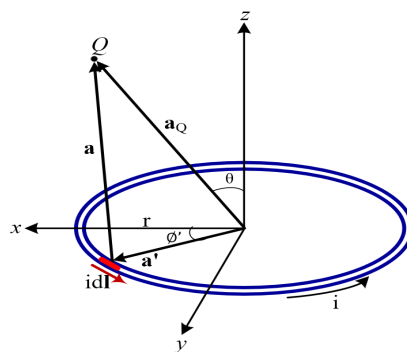


Figure 2. The symmetry axis magnetic field due to a circular current loop.

Using (1), the magnetic field contribution of the current element idl at Q can be expressed as:

$$d\mathbf{B} = \frac{\mu_0 i}{4\pi} \frac{d\mathbf{l} \times \hat{\mathbf{a}}}{a^2} = \frac{\mu_0 i}{4\pi} \frac{d\mathbf{l} \times \mathbf{a}}{a^3} = \frac{\mu_0 i r}{4\pi} \frac{z \cos\vartheta' \hat{\mathbf{i}} + z \sin\vartheta' \hat{\mathbf{j}} + (r - y \sin\vartheta') \hat{\mathbf{k}}}{(r^2 + y^2 + z^2 - 2yr \sin\vartheta')^{3/2}} d\vartheta', \quad (4)$$

where:

$$idl = r d\vartheta' (-\sin\vartheta' \hat{\mathbf{i}} + \cos\vartheta' \hat{\mathbf{j}}) : \text{the differential current element} \quad (5)$$

$$\mathbf{a}' = r(\cos\vartheta' \hat{\mathbf{i}} + \sin\vartheta' \hat{\mathbf{j}}) \quad (6)$$

$$\mathbf{a}_Q = y\hat{\mathbf{j}} + z\hat{\mathbf{k}}$$

$$\mathbf{a} = \mathbf{a}_Q - \mathbf{a}' = -r \cos\vartheta' \hat{\mathbf{i}} + (y - r \sin\vartheta') \hat{\mathbf{j}} + z\hat{\mathbf{k}} \quad (7)$$

$$a = |\mathbf{a}| = \sqrt{(-r \cos\vartheta')^2 + (y - r \sin\vartheta')^2 + z^2} = \sqrt{r^2 + y^2 + z^2 - 2yr \sin\vartheta'} \quad (8)$$

$$\hat{\mathbf{a}} = \frac{\mathbf{a}}{a} = \frac{\mathbf{a}_Q - \mathbf{a}'}{|\mathbf{a}_Q - \mathbf{a}'|} \quad (9)$$

$$d\mathbf{l} \times \hat{\mathbf{a}} = |\mathbf{a}| r d\vartheta' (-\sin\vartheta' \hat{\mathbf{i}} + \cos\vartheta' \hat{\mathbf{j}}) \times \left[-r \cos\vartheta' \hat{\mathbf{i}} + (y - r \sin\vartheta') \hat{\mathbf{j}} + z\hat{\mathbf{k}} \right] \quad (10)$$

$$= r d\vartheta' \left[z \cos\vartheta' \hat{\mathbf{i}} + z \sin\vartheta' \hat{\mathbf{j}} + (r - y \sin\vartheta') \hat{\mathbf{k}} \right] \cdot \mu \quad (11)$$

Thus, magnetic field at Q is:

$$\mathbf{B}(0, y, z) = \frac{\mu_0 i r}{4\pi} \int_0^{2\pi} \frac{z \cos\vartheta' \hat{\mathbf{i}} + z \sin\vartheta' \hat{\mathbf{j}} + (r - y \sin\vartheta') \hat{\mathbf{k}}}{(r^2 + y^2 + z^2 - 2yr \sin\vartheta')^{3/2}} d\vartheta' \quad (12)$$

The x -component of \mathbf{B} can be readily shown to be zero:

$$B_x = \frac{\mu_0 i r z}{4\pi} \int_0^{2\pi} \frac{\cos\vartheta' d\vartheta'}{(r^2 + y^2 + z^2 - 2yr \sin\vartheta')^{3/2}} = 0 \quad (13)$$

with the changing of the variable $r^2 + y^2 + z^2 - 2yr \sin\vartheta'$, the y and the z components of \mathbf{B} can be expressed as follows:

$$B_y = \frac{\mu_0 i r z}{4\pi} \int_0^{2\pi} \frac{\sin\vartheta' d\vartheta'}{(r^2 + y^2 + z^2 - 2yr \sin\vartheta')^{3/2}} \quad (14)$$

$$B_z = \frac{\mu_0 i r}{4\pi} \int_0^{2\pi} \frac{(r - y \sin\vartheta') d\vartheta'}{(r^2 + y^2 + z^2 - 2yr \sin\vartheta')^{3/2}} \quad (15)$$

From the symmetry, every point (Q) in any-plane (see Figure 2) with the same z and a_Q around the circular loop coil has equal B_z value. With this principle, B_z can be calculated for any arbitrary point at $x \neq 0$ using the equivalent value of B_z for arbitrary points in the yz -plane. Therefore, the magnetic field from a circular coil at an arbitrary point can be obtained. In case of array coils, the magnetic field at an arbitrary point from an array coil is the total number of magnetic field contributions from all single circular coils in the array coil pattern.

In [15,19,20], the magnetic field at an arbitrary point from a circular coil also can be obtained with a different approach. In the Smythe's textbook, the magnetic field is derived from the vector potential.

The vector potential A of the circular loop current at point S (Figure 3) in the cylindrical coordinate system is given by

$$A_{\varnothing} = \frac{\mu i}{4\pi} \int \frac{d\mathbf{l}}{r} = \frac{\mu i r}{4\pi} \int_0^{\pi} \frac{\cos \varnothing d\varnothing}{(r^2 + p^2 + z^2 - 2rp\cos\varnothing)^{\frac{1}{2}}} \tag{16}$$

where r = the coil radius, p = displacement in horizontal direction and z = displacement in vertical direction in cylindrical coordinate system.

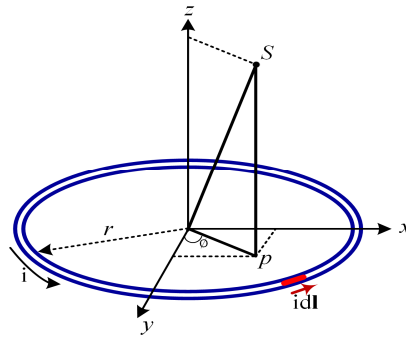


Figure 3. The magnetic field in a circular current loop.

By substituting \varnothing by $\pi + 2\theta$ with complete elliptic integrals of K and E , magnetic field component in vertical direction can be presented as:

$$H_z = \frac{1}{\mu_0} \frac{\mu i}{2\pi} \frac{1}{[(r+p)^2 + z^2]^{\frac{1}{2}}} \times \left[K(k) + \frac{r^2 - p^2 - z^2}{(r-p)^2 + z^2} E(k) \right] \tag{17}$$

$$K(k) = \int_0^{\frac{\pi}{2}} \frac{d\theta}{\sqrt{1 - k^2 \sin^2 \theta}} \tag{18}$$

$$E(k) = \int_0^{\frac{\pi}{2}} \sqrt{1 - k^2 \sin^2 \theta} d\theta \tag{19}$$

The vertical direction magnetic field can be calculated from the vector potential:

$$\mu_0 H_z = B_z \tag{20}$$

2.3. Analysis and Evaluation Method

The vertical magnetic field distribution is simulated and analyzed using a numerical method based on the off-symmetrical axis magnetic field formulation due to a circular current loop. The numerical method is derived from the Bio-Savart law as proposed in Section 2.2. The evaluated coil geometry is a circular flat spiral air-core coil shown in Figure 4.

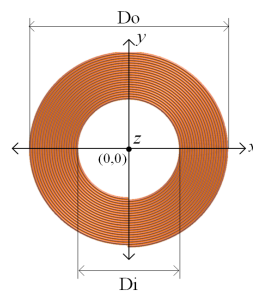


Figure 4. Circular flat spiral air core single coil geometry.

Two kind evaluation scenarios are applied to the proposed analysis and evaluation method to evaluate the array coil model vertical magnetic field distribution. The scenarios are described as follows:

- (1) In the first scenario, the vertical magnetic field distribution of single coil model with different coil parameter is analysed and evaluated. The vertical magnetic field distribution characteristic of single coil evaluation result is used to define the evaluation criteria for analyses and evaluation of the array coil models vertical magnetic field distribution. The vertical direction evaluation distance is defined at 2.5 mm from the coil surface with a unit current at 1 Ampere. The array coil model vertical magnetic field distribution is analyzed and evaluated with a variation in distances between the adjoining coil centers to meet the vertical magnetic field uniform distribution with the transmitting area as wide as possible. The evaluation criteria used in this paper is proposed as follows:
 - (a) Average vertical magnetic field resultant is not less than 60% single coil vertical magnetic field peak, and
 - (b) Magnetic field effective transmitting area is as wide as possible.

The optimal array coil pattern must comply with all criteria variables above. The array coil model evaluation is applied with different coil parameters (number of turns, inner diameter, outer diameter, pitch and wire diameter) and variety in the distance between the adjoining coil centers.

- (2) The second scenario is a case study. The general investigation result from the first evaluation scenario is applied in the array coil model design. In this evaluation scenario, different array coil model patterns which are composed of 2, 3, 4, and 6 coils are constructed from identical circular flat spiral air-core coils with given coil parameters. The vertical magnetic field distribution is analyzed and evaluated using the proposed method as described in first evaluation scenario with variety in the distance between the adjoining coil centers. The goal evaluation in this case study is recommended array coil model with close to uniform vertical magnetic field distribution and widely effective transmitting area. The array coil model patterns are shown in Figure 5.

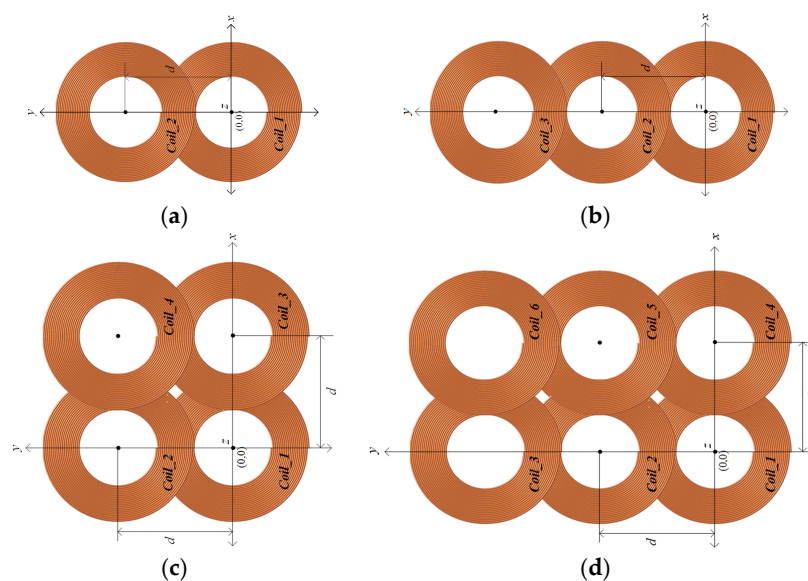


Figure 5. Single layer array coil pattern arrangements: (a) the 1×2 coil pattern; (b) the 1×3 coil pattern; (c) the 2×2 coil pattern; (d) the 2×3 coil pattern.

3. Numerical Evaluation of the Vertical Magnetic Field Distribution

3.1. The Coil with Different Coil Parameter

Two circular flat spiral air-core coil models were considered with coil parameters as shown in Table 1. These parameters were used to compute vertical magnetic field distribution in both single and array coil models. Two coil model have same outer diameter, distance between coil wire (pitch), and wire diameter but different in number of turns and inner diameter.

Table 1. Coil parameters of group_1.

| Parameter | Coil_1.1 | Coil_1.2 |
|--------------------------|----------|----------|
| Number of turns (N) | 23 | 8 |
| Inner diameter (Di) (mm) | 10 | 30 |
| Outer diameter (Do) (mm) | 40 | 40 |
| Pitch (P) (mm) | 0.03 | 0.03 |
| Wire diameter (W) (mm) | 0.643 | 0.643 |

The single coil magnetic field distribution calculation and evaluation was first addressed and then followed with array coil models. The vertical magnetic field distribution of single coil is numerically calculated along the y-axis to obtain the magnetic field off-symmetry axis due to the circular current loop. The evaluation path in the y-axis direction is shown in Figure 6.

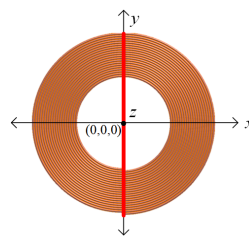


Figure 6. The Single coil evaluation path.

The vertical magnetic field (B_z) distribution calculation and characteristic of single coil (Coil_1.1) with $D_i = 10$ mm and $N = 8$ is presented in Figure 7a.

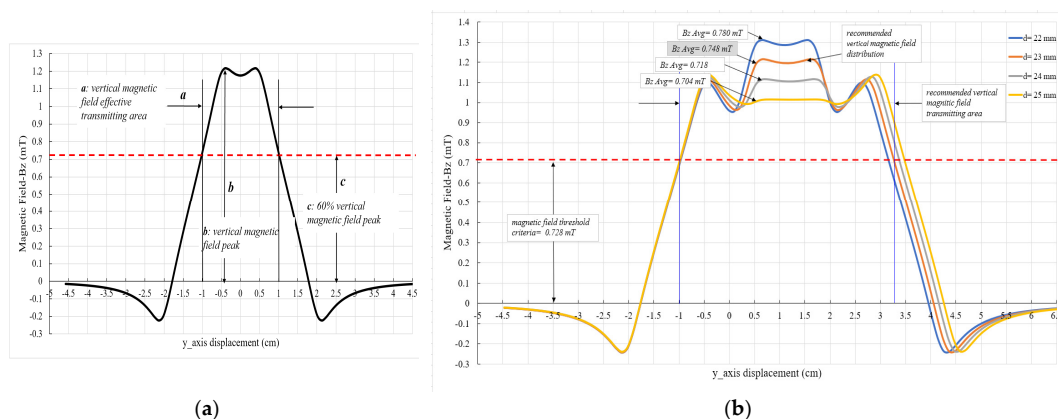


Figure 7. Vertical magnetic field (B_z) distribution characteristic curve along the y-axis: (a) single coil with $D_i = 10$ mm, $D_o = 40$ mm, and $N = 23$ turns, (b) 1×2 array coil composed of two identical single coils ($D_i = 10$ mm, $D_o = 40$ mm, and $N = 23$ turns) with a variation in the distances between the adjoining coil centers (d).

As shown in Figure 7a, the vertical magnetic field peak ($B_z \text{ max}$) = 1.214 mT, and 60% $B_z \text{ max}$ = 0.728 mT. While the horizontal length of the vertical magnetic field effective transmitting area = 20 mm.

The array coil model magnetic field distribution calculation and evaluation were conducted with the number of coils at 2 (the 1×2 array coil pattern). The coil model and the evaluation path in the y-axis direction is shown in Figure 8.

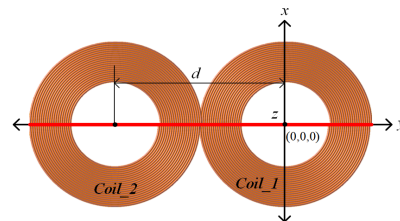


Figure 8. The 1×2 array coil evaluation path.

Figure 7b presents the vertical magnetic field (B_z) distribution calculation and characteristic of the 1×2 array coil model composed of two identical coils with $D_i = 10$ mm and $N = 23$. The evaluation was performed with variety of distances between the adjoining coil centers (d) at 22 mm, 23 mm, 24 mm, and 25 mm. The magnetic field threshold criteria were derived from magnetic field distribution characteristic in Figure 7a. It is equal to 60% $B_z \text{ max}$ = 0.728 mT. From the evaluation result as shown in Figure 7b, the characteristic curve has the vertical magnetic field average ($B_z \text{ Avg}$) = 0.748 mT, the horizontal length of the vertical magnetic field effective transmitting area = 50 mm, and the distance between the adjoining coil centers (d) at 23 mm was a recommended vertical magnetic field distribution for 1×2 array coil model with coil $D_i = 10$ mm, coil $D_o = 40$ mm, and $N = 23$ turns.

The second coil (Coil_1.2) with $D_i = 30$ mm and $N = 8$ also was evaluated using the same method described in the first coil (Coil_1.1) evaluation. The evaluation result is shown in Figure 9.

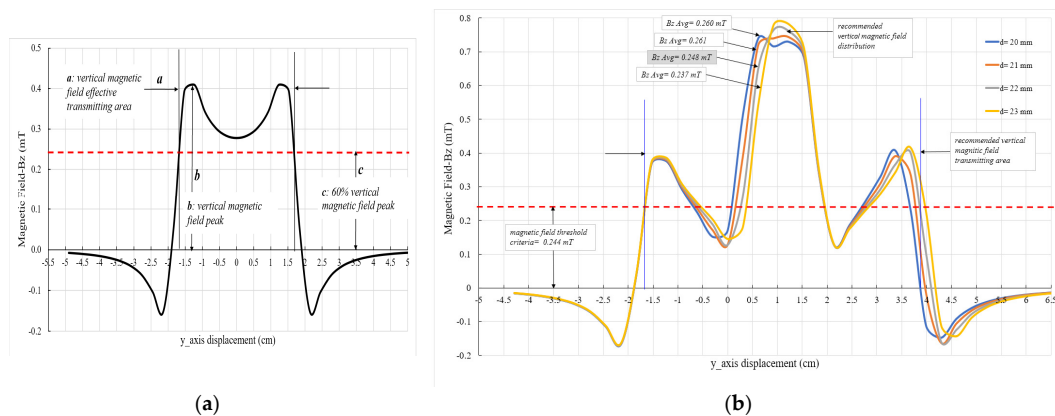


Figure 9. Vertical magnetic field (B_z) distribution characteristic curve along the y-axis: (a) single coil with $D_i = 30$ mm, $D_o = 40$ mm and $N = 8$ turns, (b) 1×2 array coil composed of two identical single coils ($D_i = 30$ mm, $D_o = 40$ mm, and $N = 8$ turns) with a variation in the distances between the adjoining coil centers (d).

Figure 9a describes the calculation and evaluation result for single coil (Coil_1.2) with $D_i = 30$ mm and $D_o = 40$ mm. The vertical magnetic field peak ($B_z \text{ max}$) = 0.408 mT, and 60% $B_z \text{ max}$ = 0.244 mT. While the horizontal length of the vertical magnetic field effective transmitting area = 35 mm.

The vertical magnetic field (B_z) distribution calculation and characteristic of the 1×2 array coil model composed of Coil_1.2 is presented in Figure 9b. The evaluation was performed with a variety of distance between the adjoining coil centers (d) at 20 mm, 21 mm, 22 mm, and 23 mm. The magnetic field threshold criteria were derived from the magnetic field distribution characteristic in Figure 9a. It is

equal with $60\% B_z \text{ max} = 0.244 \text{ mT}$. The characteristic curve has the vertical magnetic field average ($B_z \text{ Avg}$) = 0.248 mT , the horizontal length of the vertical magnetic field effective transmitting area = 55 mm , and the distance between the adjoining coil centers (d) at 22 mm was a recommended vertical magnetic field distribution for 1×2 array coil model with coil $D_i = 30 \text{ mm}$, coil $D_o = 40 \text{ mm}$, and $N = 8$ turns.

The evaluation was continued with different coils that have coil parameters as shown in Table 2. These coils have the outer diameter larger than the two previous coils (Coil_1.1 and Coil_1.2). Coil_2.1 and Coil_2.2 have the same outer diameter, distance between coil wire (pitch), and wire diameter but different in number of turns and inner diameter.

Table 2. Coil parameters of group_2.

| Parameter | Coil_2.1 | Coil_2.2 |
|--------------------------|----------|----------|
| Number of turns (N) | 37 | 15 |
| Inner diameter (Di) (mm) | 20 | 40 |
| Outer diameter (Do) (mm) | 60 | 60 |
| Pitch (P) (mm) | 0.03 | 0.03 |
| Wire diameter (W) (mm) | 0.643 | 0.643 |

The second coil group (Coil_2.1 and Coil_2.2) was also evaluated using the same method described in the first coil group evaluation. The evaluation results are shown in Figures 10 and 11.

Figure 10a describes the calculation and evaluation result for single coil (Coil_2.1) with $D_i = 20 \text{ mm}$ and $D_o = 60 \text{ mm}$. The vertical magnetic field peak ($B_z \text{ max}$) = 1.339 mT , and $60\% B_z \text{ max} = 0.803 \text{ mT}$. While the horizontal length of the vertical magnetic field effective transmitting area = 35 mm .

The vertical magnetic field (B_z) distribution calculation and characteristic of the 1×2 array coil pattern which composed of Coil_2.1 is presented in Figure 10b. The evaluation was performed with variety of distance between the adjoining coil centers (d) at $36, 37, 38$ and 39 mm . The magnetic field threshold criteria is 0.244 mT . The characteristic curve has vertical magnetic field distribution with the vertical magnetic field average ($B_z \text{ Avg}$) = 0.805 mT , the horizontal length of the vertical magnetic field effective transmitting area = 72 mm , and the distance between the adjoining coil centers (d) at 38 mm was a recommended vertical magnetic field distribution for 1×2 array coil model with coil $D_i = 20 \text{ mm}$, coil $D_o = 60 \text{ mm}$, and $N = 37$ turns.

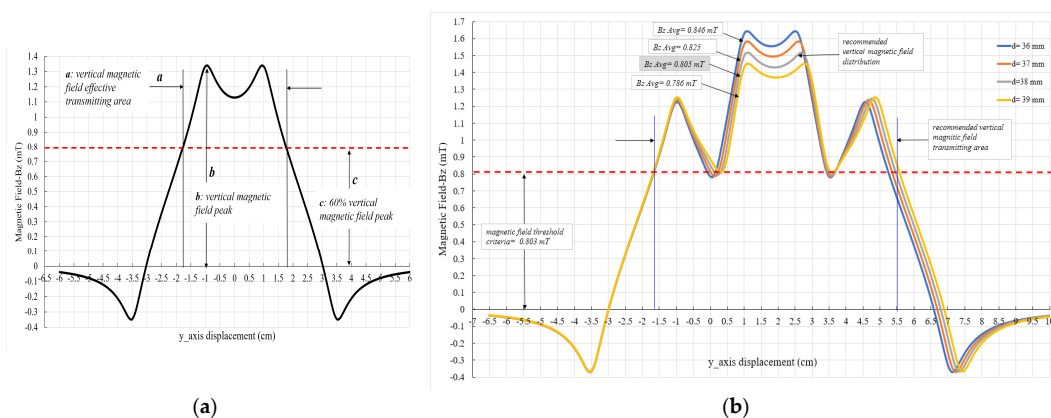


Figure 10. Vertical magnetic field (B_z) distribution characteristic curve along the y-axis: (a) single coil with $D_i = 20 \text{ mm}$, $D_o = 60 \text{ mm}$, and $N = 37$ turns, (b) 1×2 array coil composed of two identical single coils ($D_i = 20 \text{ mm}$, $D_o = 60 \text{ mm}$, and $N = 37$ turns) with a variation in the distances between the adjoining coil centers (d).

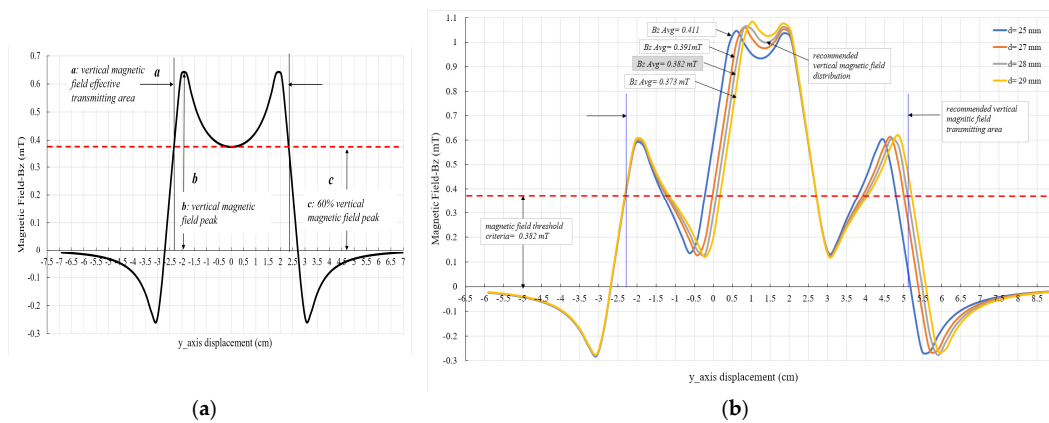


Figure 11. Vertical magnetic field (B_z) distribution characteristic curve along the y -axis: (a) single coil with $D_i = 40$ mm, $D_o = 60$ mm, and $N = 15$ turns, (b) 1×2 array coil composed of two identical single coils ($D_i = 40$ mm, $D_o = 60$ mm, and $N = 15$ turns) with a variation in the distances between the adjoining coil centers (d).

Figure 11a describes the calculation and evaluation result for single coil (Coil_2.2) with $D_i = 40$ mm and $D_o = 60$ mm. The vertical magnetic field peak ($B_z \max$) = 0.637 mT, and 60% $B_z \max$ = 0.382 mT. The horizontal length of the vertical magnetic field effective transmitting area = 45 mm.

While Figure 11b describes the vertical magnetic field (B_z) distribution calculation and characteristic of the 1×2 array coil model composed of Coil_2.2. The evaluation was performed with variety of distances between the adjoining coil centers (d) at 25 mm, 27 mm, 28 mm, and 29 mm. The magnetic field threshold criteria = 0.244 mT. The characteristic curve has vertical magnetic field distribution with the vertical magnetic field average ($B_z \text{ Avg}$) = 0.382 mT, the horizontal length of the vertical magnetic field effective transmitting area = 75 mm, and the distance between the adjoining coil centers (d) at 28 mm was a recommended vertical magnetic field distribution for 1×2 array coil model with coil $D_i = 40$ mm, coil $D_o = 60$ mm, and $N = 15$ turns.

The next evaluation was the coils in the third coil group (Coil_3.1 and Coil_3.2). The evaluation also used the same method described in the first and second group coil evaluations. The coil parameters of the third coil group is presented in Table 3. The evaluation results are shown in Figures 12 and 13.

The calculation and evaluation result for single coil (Coil_3.1) with $D_i = 30$ mm and $D_o = 80$ mm is described in Figure 12a. The vertical magnetic field peak ($B_z \max$) = 1.222 mT, and 60% $B_z \max$ = 0.733 mT. The horizontal length of the vertical magnetic field effective transmitting area = 45 mm.

The vertical magnetic field (B_z) distribution calculation and characteristic of the 1×2 array coil pattern composed of Coil_3.1 is presented in Figure 12b. The evaluation was performed with variety of distance between the adjoining coil centers (d) at 40 mm, 41 mm, 42 mm, and 43 mm. The magnetic field threshold criteria = 0.733 mT. The vertical magnetic field distribution characteristic curve with the vertical magnetic field average ($B_z \text{ Avg}$) = 0.731 mT, the horizontal length of the vertical magnetic field effective transmitting area = 85 mm, and the distance between the adjoining coil centers (d) at 42 mm was recommended vertical magnetic field distribution for 1×2 array coil model with coil $D_i = 30$ mm, coil $D_o = 80$ mm, and $N = 38$ turns.

Figure 13a describes the calculation and evaluation result for single coil (Coil_3.2) with $D_i = 45$ mm and $D_o = 80$ mm. The vertical magnetic field peak ($B_z \max$) = 0.916 mT, and 60% $B_z \max$ = 0.549 mT. The horizontal length of the vertical magnetic field effective transmitting area = 50 mm.

While the vertical magnetic field (B_z) distribution calculation and characteristic of the 1×2 array coil pattern composed of Coil_3.2 is presented in Figure 13b. The evaluation was performed with a variety of distance between the adjoining coil centers (d) at 34 mm, 35 mm, 36 mm, and 37 mm. The magnetic field threshold criteria = 0.549 mT. The vertical magnetic field distribution with the vertical magnetic field average ($B_z \text{ Avg}$) = 0.567 mT, the horizontal length of the vertical magnetic field

effective transmitting area = 90 mm, and the distance between the adjoining coil centers (d) at 36 mm was recommended vertical magnetic field distribution for 1 × 2 array coil model with coil Di = 45 mm, coil Do = 80 mm, and N = 23 turns.

The magnetic field distribution numerical calculation and evaluation was also conducted on other single and array coils with a variety of inner diameters, outer diameters, number of turns, and different array coil model patterns (2 × 2, 2 × 3, 2 × 6, 4 × 4).

Table 3. Coil parameters of group_3.

| Parameter | Coil_3.1 | Coil_3.2 |
|--------------------------|----------|----------|
| Number of turns (N) | 38 | 23 |
| Inner diameter (Di) (mm) | 30 | 45 |
| Outer diameter (Do) (mm) | 80 | 80 |
| Pitch (P) (mm) | 0.03 | 0.03 |
| Wire diameter (W) (mm) | 0.643 | 0.643 |

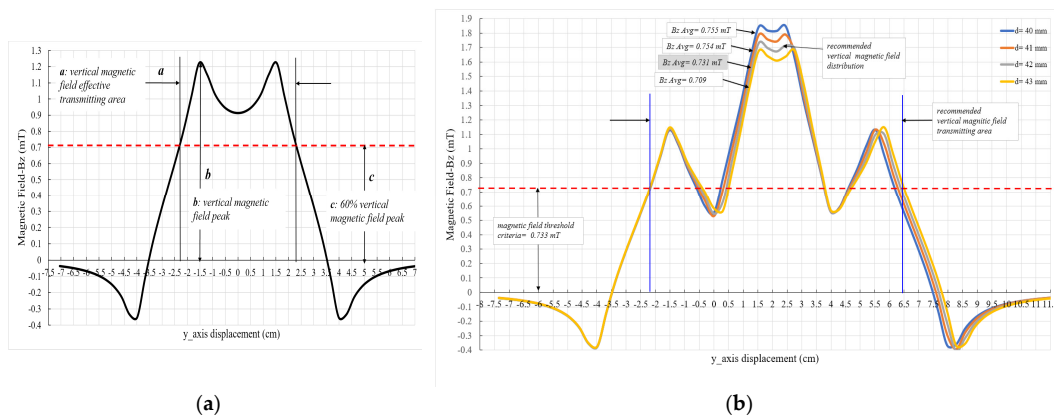


Figure 12. Vertical magnetic field (Bz) distribution characteristic curve along the y-axis: (a) single coil with Di = 30 mm, Do = 80 mm, and N = 38 turns, (b) 1 × 2 array coil composed of two identical single coils (Di = 30 mm, Do = 80 mm, and N = 38 turns) with a variation in the distances between the adjoining coil centers (d).

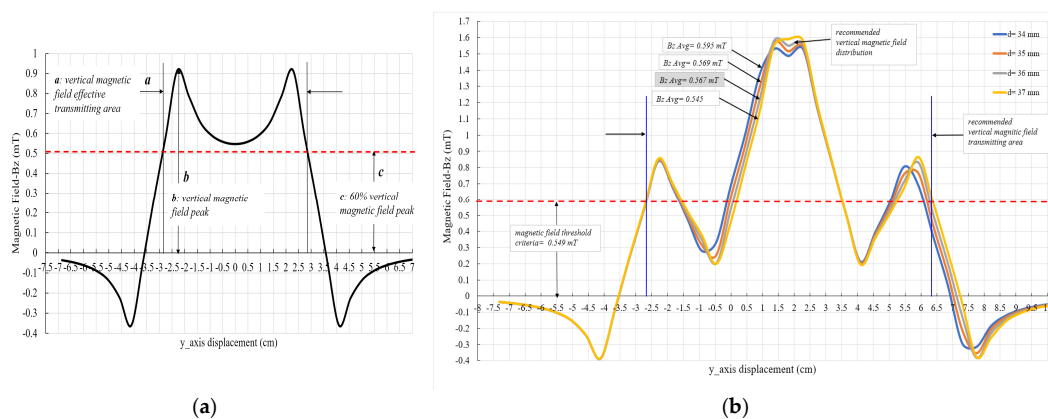


Figure 13. Vertical magnetic field (Bz) distribution characteristic curve along the y-axis: (a) single coil with Di = 45 mm, Do = 80 mm, and N = 23 turns, (b) 1 × 2 array coil composed of two identical single coils (Di = 45 mm, Do = 80 mm, and N = 23 turns) with a variation in the distances between the adjoining coil centers (d).

3.2. Discussion

The vertical magnetic field distribution and effective transmitting area of the evaluated single or array coils were examined following the evaluation criteria is described in Section 2.3. In the case of the coil which has the coil parameters as presented in Tables 1–3, the array coil models generate a wider horizontal transmitting area than the single coil along the y-axis direction. At the evaluated (recommended) distance between the adjoining coil centers (d), the array coil models also generate close to uniform vertical magnetic field distribution average at the level which the single coil generates a magnetic field at 60% of its magnetic field peak.

From the magnetic field distribution characteristic curve evaluation result, the distance between the adjoining coil centers (d) and outer coil diameter (D_o) impact significant effect upon the evaluated array coil model vertical magnetic field distribution. The evaluation result is shown in Figures 7 and 9–13. The comparison evaluation result is summarized in Table 4.

Table 4. Comparison evaluation result.

| Coil Parameters | 60%Bz-Peak/Bz Avg (mT) | | The Width of Transmitting Area (mm) | | The Distance between the Adjoining Coil Center (mm) |
|--------------------------------|------------------------|------------------|-------------------------------------|------------------|---|
| | Single Coil | 1 × 2 Array Coil | Single Coil | 1 × 2 Array Coil | 1 × 2 Array Coil |
| Di = 10 mm, Do = 40 mm, N = 23 | 0.728 | 0.748 | 20 | 50 | 23 |
| Di = 30 mm, Do = 40 mm, N = 8 | 0.244 | 0.248 | 35 | 55 | 22 |
| Di = 20 mm, Do = 60 mm, N = 37 | 0.803 | 0.805 | 35 | 72 | 38 |
| Di = 40 mm, Do = 60 mm, N = 15 | 0.382 | 0.382 | 45 | 75 | 28 |
| Di = 30 mm, Do = 80 mm, N = 38 | 0.733 | 0.733 | 45 | 85 | 42 |
| Di = 45 mm, Do = 80 mm, N = 23 | 0.549 | 0.567 | 50 | 90 | 36 |

The evaluation and investigation of other single coils and array coil model patterns with different coil parameters also presented a similar result pattern to that shown in Table 4.

From Table 4, the distance between the adjoining coil centers (d) in the array coil model can be defined close to the half coil outer diameter ($1/2D_o$) to generate close to uniform vertical magnetic field distribution.

4. Case Study

The circular flat spiral air-core coil with coil parameters as described in Table 5 was examined in order to generate uniform vertical magnetic field distribution in the form of array coil model.

Table 5. Coil parameters of case study.

| Parameter | Single Coil |
|--------------------------|-------------|
| Number of turns (N) | 17 |
| Inner diameter (Di) (mm) | 25 |
| Outer diameter (Do) (mm) | 47.8 |
| Pitch (P) (mm) | 0.03 |
| Wire diameter (W) (mm) | 0.643 |

In this case study, the coil geometry was chosen with considering the coil usage in wireless power charger applications. The numerical calculation and evaluation results are presented in the following subsections.

4.1. Single Coil Evaluation

The characteristic curve of a single coil vertical magnetic field is shown in Figure 14a. The vertical magnetic field peak (B_z max) along the y-axis is 0.804 mT and the 60% vertical magnetic field peak is 0.482 mT. The 60% single coil vertical magnetic field peak is the proposed value to obtain the vertical magnetic field effective transmitting area to meet the uniform vertical magnetic field distribution. The horizontal length of the vertical magnetic field effective transmitting area = 45 mm. The overall single coil vertical magnetic field distribution is shown in Figure 14b. The magnetic field effective transmitting area is plotted on that distribution based on Figure 14a.

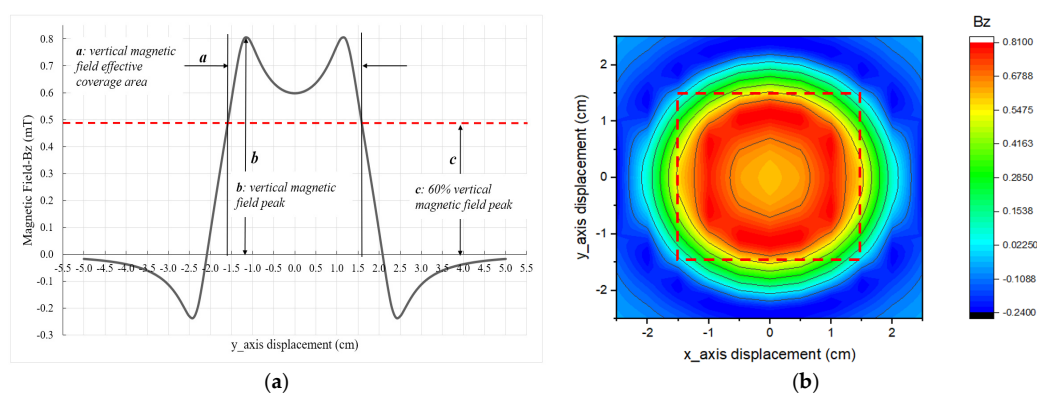


Figure 14. Single coil vertical magnetic field (B_z) characteristic: (a) distribution curve along the y-axis, (b) overall vertical magnetic field (B_z) distribution and magnetic field effective transmitting area.

4.2. The Two Coils Pattern Evaluation

The evaluation path in the y-axis direction of the 1×2 array coil pattern is shown in Figure 15.

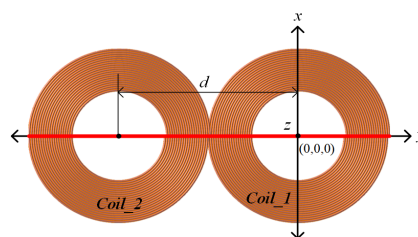


Figure 15. The 1×2 array coil evaluation path.

The distance between the adjoining coil centers (d) of the 1×2 array coil is arranged at 50 mm based on the single coil characteristic curve in Figure 14a. The 1×2 array coil vertical magnetic field characteristic curve is shown in Figure 16a, and the vertical magnetic field average (B_z Avg) resultant for this pattern along the y-axis is 0.291 mT.

The magnetic field evaluation of this pattern was performed using the difference in the distance between the adjoining coil centers (d) at 20 mm, 25 mm, 26 mm, 27 mm, 28 mm, and 30 mm respectively. The vertical magnetic field distribution numerical calculation results in the characteristic curve are shown in Figure 16b. The characteristic curve shows that the vertical magnetic field distribution with the vertical magnetic field average (B_z Avg) = 0.494 mT, the horizontal length of the vertical magnetic field effective transmitting area = 57 mm, and the distance between the adjoining coil centers (d) at 26 mm was the recommended vertical magnetic field distribution for the 1×2 array coil model.

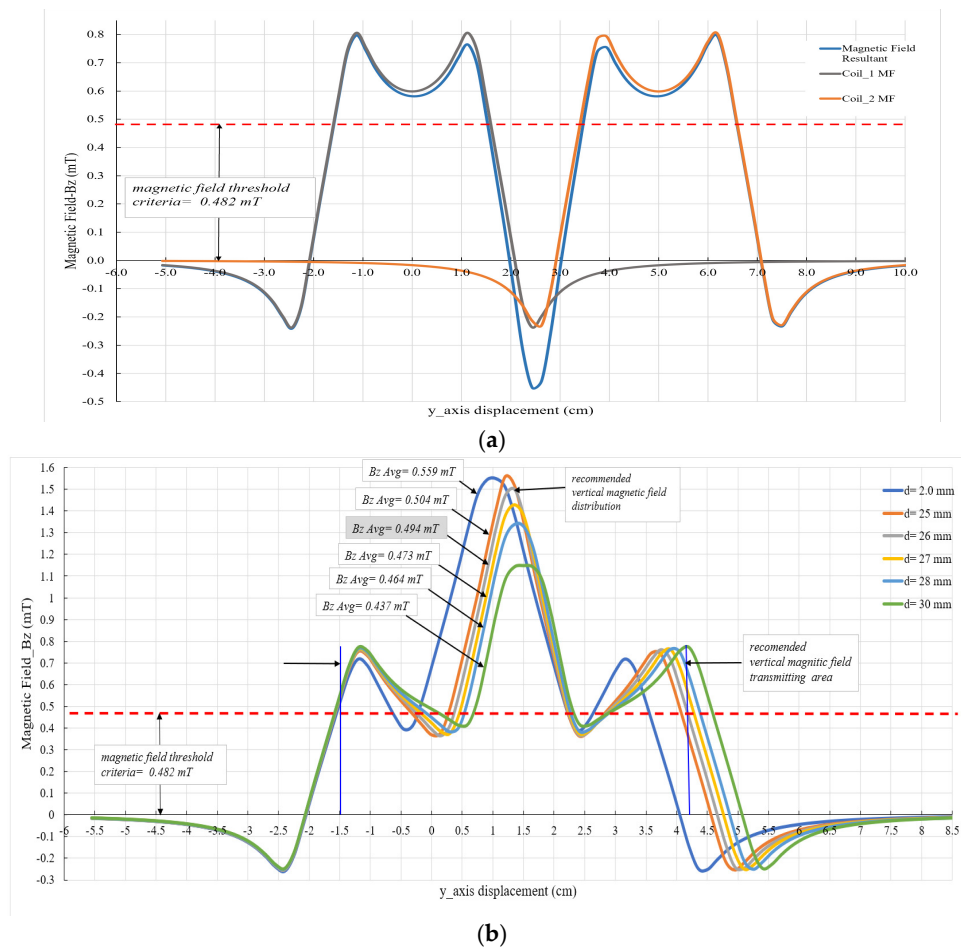


Figure 16. The characteristic curve of 1×2 array coil vertical magnetic field (B_z) distribution along the y-axis: (a) with the distance between the adjoining coil centers (d) at 50 mm, (b) with a variation in the distances between the adjoining coil centers.

4.3. The Three Coils Pattern Evaluation

The evaluation path in the y-axis direction of the 1×3 array coil pattern is shown in Figure 17.

In this analysis, the distance between the adjoining coil centers (d) of the 1×3 array coil was arranged at 26 mm. This refers to the 1×2 array coil pattern which generates the vertical magnetic field average (B_z Avg) resultant more than magnetic field threshold criteria (0.482 mT). The 1×3 array coil vertical magnetic field characteristic curve is shown in Figure 18a and the vertical magnetic field average (B_z Avg) resultant for this pattern at $x = 0$ is 0.543 mT.

This array coil model was also evaluated with the difference in the distance between the adjoining coil centers (d) at 26 mm, 28 mm, 30 mm, 31 mm, and 32 mm respectively. The vertical magnetic field distribution numerical calculation results in the characteristic curve as shown in Figure 18b.

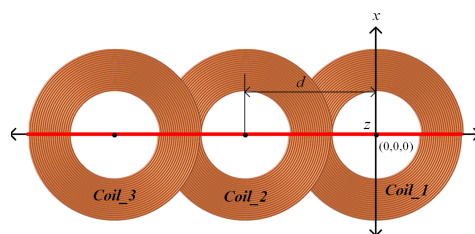


Figure 17. The 1×3 array coil evaluation path.

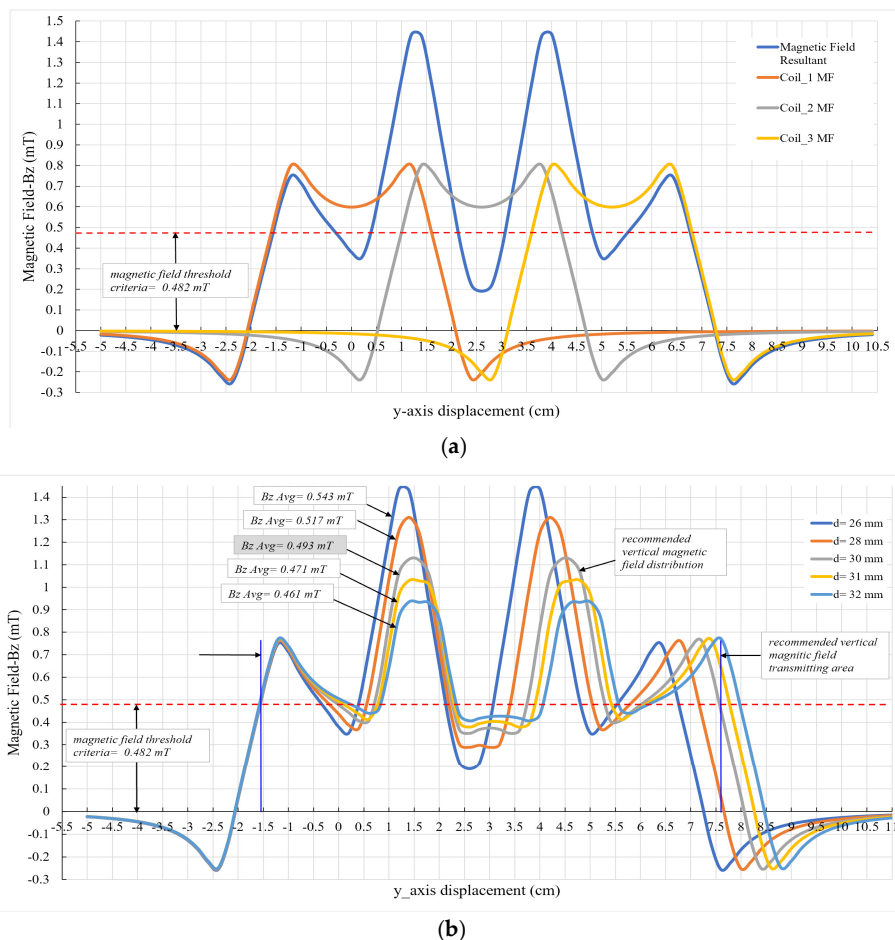


Figure 18. The characteristic curve of 1×3 array coil vertical magnetic field (B_z) distribution along the y-axis: (a) with the distance between the adjoining coil centers (d) at 26 mm, (b) with a variation in the distances between the adjoining coil centers.

The characteristic curve shows that the vertical magnetic field distribution with the vertical magnetic field average ($B_z \text{ Avg}$) = 0.493 mT, the horizontal length of the vertical magnetic field effective transmitting area = 90 mm, and the distance between the adjoining coil centers (d) at 30 mm was the recommended vertical magnetic field distribution for 1×3 array coil model.

4.4. The Four Coils Pattern

The evaluation path in the y-axis direction for the 2×2 array coil vertical magnetic field distribution is shown in Figure 19.

The distance between the adjoining coil centers (d) of the 2×2 array coil is arranged at 26 mm. This refers to the 1×2 array coil pattern which generates the vertical magnetic field average ($B_z \text{ Avg}$) resultant more than the magnetic field threshold criteria (0.482 mT). The 2×2 array coil vertical magnetic field characteristic curve is shown in Figure 20a, and the vertical magnetic field average ($B_z \text{ Avg}$) resultant for this pattern is 0.599 mT.

This pattern evaluated with the difference in the distance between the adjoining coil centers (d) at 26 mm, 26.5 mm, 27 mm, 27.5 mm, and 28 mm respectively. The vertical magnetic field distribution numerical calculation results in the characteristic curve are shown in Figure 20b. The characteristic curve shows that the vertical magnetic field distribution with the vertical magnetic field average ($B_z \text{ Avg}$) = 0.487 mT, the horizontal length of the vertical magnetic field effective transmitting area = 52 mm, and the distance between the adjoining coil centers (d) at 27.5 mm was the recommended vertical magnetic field distribution for 2×2 array coil model.

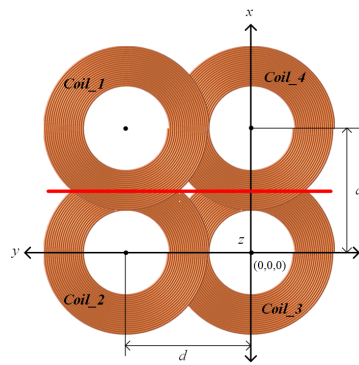


Figure 19. The 2 × 2 array coil evaluation path.

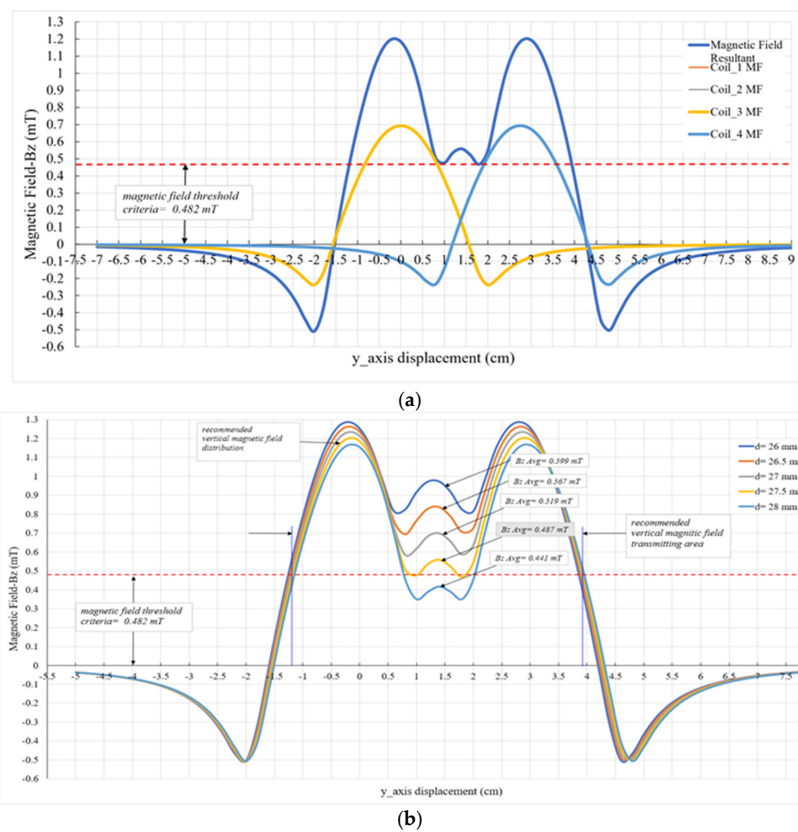


Figure 20. The characteristic curve of 2 × 2 array coil vertical magnetic field (Bz) distribution along the y-axis direction at the center of the distance between the adjoining coil centers (d): (a) with the distance between the adjoining coil centers at 26 mm, (b) with a variation in the distances between the adjoining coil centers.

4.5. The Six Coils Pattern

The evaluation path in the y-axis direction of the 2 × 3 array coil pattern is shown in Figure 21.

Based on the 1 × 2 array coil pattern, the distance between the adjoining coil centers (d) of this array coil pattern is arranged at 26 mm. The vertical magnetic field characteristic curve is shown in Figure 22a with the vertical magnetic field average (Bz Avg) resultant along the y-axis direction is 0.640 mT. This pattern evaluated with the difference in the distance between the adjoining coil centers (d) at 26 mm, 27 mm, 27.5 mm, and 28 mm respectively.

The numerical calculation results of vertical magnetic field distribution in the characteristic curve is shown in Figure 22b. The characteristic curve shows that the vertical magnetic field distribution with

the vertical magnetic field average ($B_z \text{ Avg}$) = 0.506 mT, the horizontal length of the vertical magnetic field effective transmitting area = 79 mm, and the distance between the adjoining coil centers (d) at 27.5 mm is the recommend array coil.

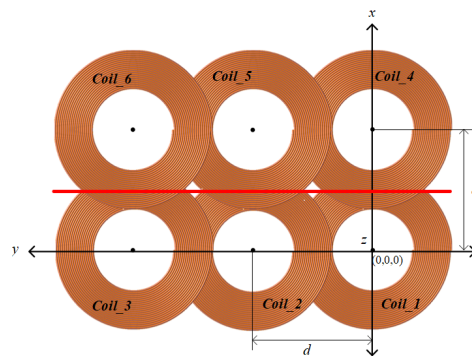


Figure 21. The 2×3 array coil evaluation path.

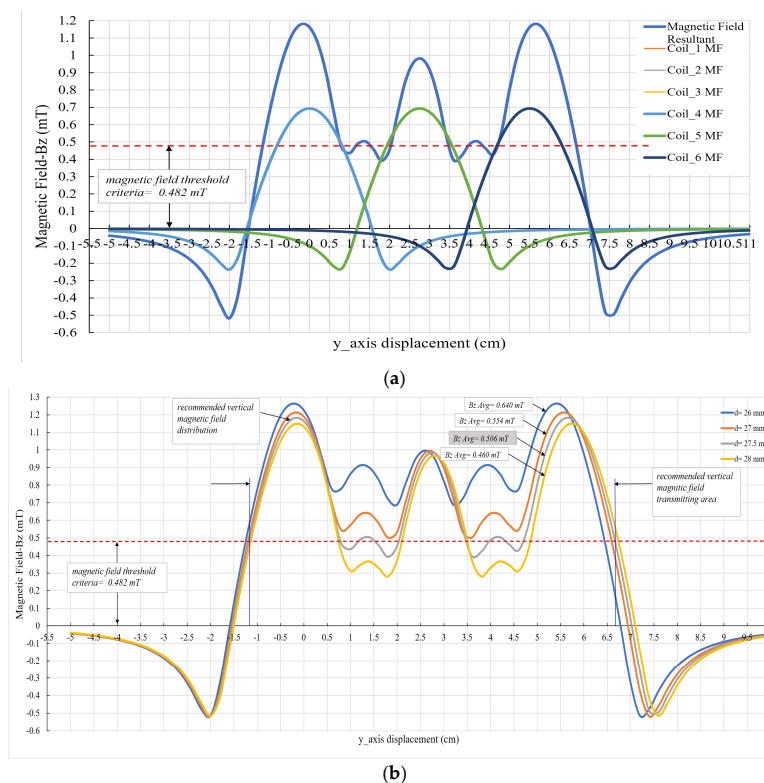


Figure 22. The characteristic curve of 2×3 array coil vertical magnetic field distribution along the y-axis direction at the center of the distance between the adjoining coil centers: (a) with the distance between the adjoining coil centers (d) at 26 mm, (b) with a variation in the distances between the adjoining coil centers.

4.6. Discussion

According to the result investigation in Section 3, the array coil model patterns were analyzed and evaluated with the variety of distance between the adjoining coil centers close to 24 mm (outer coil diameter is 47.8 mm).

The numerical analysis and evaluation results of 1×2 , 1×3 , 2×2 , and 2×3 array coil model patterns are shown in Figure 16b, Figure 18b, Figure 20b, and Figure 22b. Based on the analysis method presented in Sections 2.2 and 2.3, only the array coil model vertical magnetic field distribution that meet the evaluation criteria are selected to provide close to uniform vertical magnetic field

distribution. Therefore, with reference to the characteristic curves in Figure 16b, Figure 18b, Figure 20b, and Figure 22b, the 1×2 array coil model with the distance between the adjoining coil centers (d) at 26 mm, the 1×3 array coil model with $d = 30$ mm, the 2×2 array coil model with $d = 27.5$ mm, and the 2×3 array coil model with $d = 27.5$ mm are recommended array coil models that provide close to uniform vertical magnetic field distribution. Moreover, these array coil models also provide wider vertical magnetic field effective transmitting area than other array coil models with other the distance between the adjoining coil centers. The other vertical magnetic field distributions that also provide the vertical magnetic field average (B_z Avg) resultant more than the magnetic field threshold criteria are not considered because they have the vertical magnetic field effective transmitting area less than the vertical magnetic field effective transmitting area of the recommended array coil model.

The overall recommended vertical magnetic field distribution of array coil pattern models for the case study is plotted in Figure 23 including their magnetic field effective transmitting area plotting. The magnetic field effective transmitting area is plotted based on the magnetic field distribution numerical evaluation results as shown in Figure 16b, Figure 18b, Figure 20b, and Figure 22b.

Single circular flat spiral air-core array coil with the proper distance between the adjoining coil centers can provide close to uniform vertical magnetic field distribution and the wider magnetic field effective transmitting area.

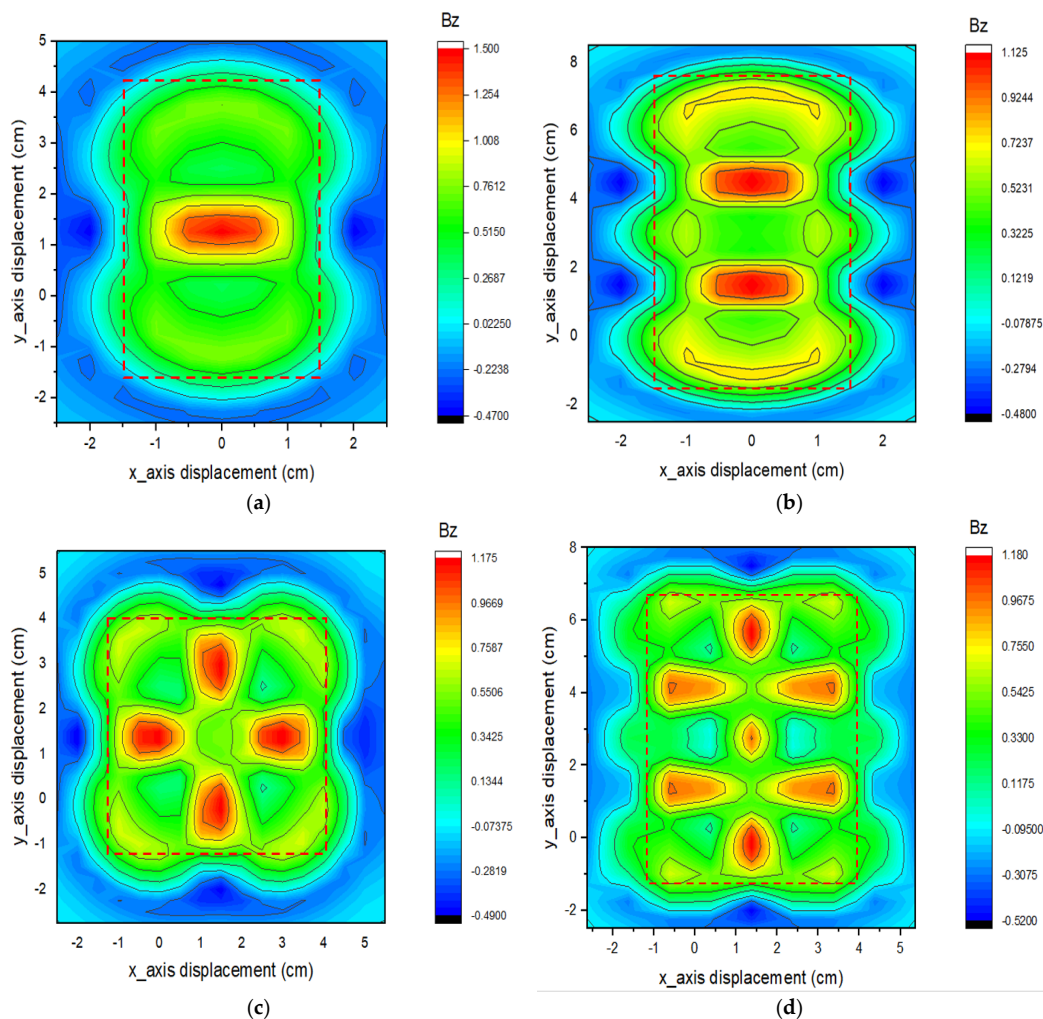


Figure 23. The recommended vertical magnetic field (B_z) distribution and the magnetic field effective transmitting area of the case study: (a) 1×2 array coil pattern, (b) 1×3 array coil pattern, (c) 2×2 array coil pattern, (d) 2×3 array coil pattern.

5. Conclusions

With the proposed magnetic field calculation and evaluation, the characteristic array coil pattern model vertical magnetic field distribution can be observed and investigated to generate close to uniform vertical magnetic field distribution.

The vertical magnetic field average (B_z Avg) resultant and vertical magnetic field effective transmitting area of array coil model with given coil parameters (inner coil diameter (D_i), outer coil diameter (D_o), wire diameter (W), pitch (P) and a number of turns (N)) changing as the effect in variation in distances between the adjoining coil centers. The proper distance between the adjoining coil centers can provide uniform vertical magnetic field distribution and the wider magnetic field effective transmitting area. The distance between the adjoining coil centers should be defined close to the half coil outer diameter ($1/2D_o$) to generate close to uniform vertical magnetic field distribution.

This evaluation method provides an easier and faster the vertical magnetic field distribution evaluation for single-layer circular flat spiral air-core $n \times m$ array coil pattern models. Moreover, it can be extended with a verifying step in practical implementation.

Author Contributions: Conceptualization, Y.-D.K.; methodology, C.B.D.K. and Y.-D.K.; formal analysis, C.B.D.K., P. and W.-J.L.; investigation, C.B.D.K., P., Y.-D.K. and W.-J.L.; supervision, Y.-D.K.; resources, Y.-D.K.; writing—original draft preparation, C.B.D.K.; writing—review and editing, W.-J.L. and Y.-D.K.

Funding: This research was funded by and the Ministry of Science and Technology of Taiwan (MOST 107-3113-E-008-003).

Acknowledgments: The authors thank the Ministry of Science and Technology of Taiwan.

Conflicts of Interest: The authors declare no conflict of interest.

References

- Jang, Y.; Jovanovic, M.M. A contactless electrical energy transmission system for portable-telephone battery chargers. *IEEE Trans. Ind. Electron.* **2003**, *50*, 520–527. [[CrossRef](#)]
- Kim, C.; Seo, D.; You, J.; Park, J.; Cho, B. Design of a contactless battery charger for cellular phone. *IEEE Trans. Ind. Electron.* **2001**, *48*, 1238–1247.
- Choi, B.; Nho, J.; Cha, H.; Ahn, T.; Choi, S. Design and implementation of low-profile contactless battery charger using planar printed circuit board windings as energy transfer device. *IEEE Trans. Ind. Electron.* **2004**, *51*, 140–147. [[CrossRef](#)]
- Hui, S.Y.R.; Ho, W.W.C. A new generation of universal contactless battery charging platform for portable consumer electronic equipment. *IEEE Trans. Power Electron.* **2005**, *20*, 620–627. [[CrossRef](#)]
- Sakamoto, H.; Harada, K.; Washimiya, S.; Takehara, K. Large air-gap coupler for inductive charger. *IEEE Trans. Magn.* **1999**, *35*, 3526–3528. [[CrossRef](#)]
- Joung, G.B.; Cho, B.H. An energy transmission system for an artificial heart using leakage inductance compensation of transcutaneous transformer. *IEEE Trans. Power Electron.* **1998**, *13*, 1013–1022.
- Neugebauer, T.C.; Perreault, D.J. Filters with inductance cancellation using printed circuit board transformers. *IEEE Trans. Power Electron.* **2004**, *19*, 591–602. [[CrossRef](#)]
- Shiri, A.; Moghadam, D.E.; Pahlavani, M.R.A.; Shoulaie, A. Finite element-based analysis of magnetic forces between planar spiral coils. *J. Electromagn. Anal. Appl.* **2010**, *2*, 311–317. [[CrossRef](#)]
- Andris, P.; Weis, J.; Frollo, I. Magnetic field of spiral-shaped coil. In Proceedings of the 7th International Conference on Measurement, Bratislava, Institute of Measurement Science SAS, Smolenice, Slovakia, 20–23 May 2009; pp. 262–265.
- Singh, V.; Qusba, A.; Roy, A.; Castro, R.A.; McClure, K.; Dai, R.; Greenberg, R.J.; Weiland, J.D.; Humayun, M.S.; Lazzi, G. Specific absorption rate and current densities in the human eye and head induced by the telemetry link of an epiretinal prosthesis. *IEEE Trans. Antennas Propag.* **2009**, *57*, 3110–3118. [[CrossRef](#)]
- Waffenschmidt, E. Homogeneous magnetic coupling for free positioning in an inductive wireless power system. Emerging and Selected Topics in Power Electronics. *IEEE J. Emerg. Sel. Top. Power Electron.* **2015**, *3*, 226–233. [[CrossRef](#)]

12. Minnaert, B.; Stevens, N. An improved algorithm for the creation of homogeneous magnetic field distributions. In Proceedings of the 2015 International Conference on Electromagnetics in Advanced Applications (ICEAA), Turin, Italy, 7–11 September 2015; pp. 517–520.
13. Azpúra, M.A. A semi-analytical method for the design of coil-systems for homogeneous magnetostatic field generation. *Prog. Electromagn. Res. B* **2012**, *37*, 171–189. [[CrossRef](#)]
14. Minnaert, B.; Strycker, L.D.; Stevens, N. Design of a Planar, Concentric Coil for the Generation of a Homogeneous Vertical Magnetic Field Distribution. *ACES J.* **2017**, *32*, 1056–1063.
15. Nguyen, M.Q.; Hughes, Z.; Woods, P.; Seo, Y.-S.; Rao, S.; Chiao, J.-C. Field Distribution Models of Spiral Coil for Misalignment Analysis in Wireless Power Transfer Systems. *IEEE Trans. Microw. Theory Tech.* **2014**, *62*, 920–930. [[CrossRef](#)]
16. Cortes, I.; Kim, W.-J. Lateral Position Error Reduction Using Misalignment-Sensing Coils in Inductive Power Transfer Systems. *IEEE/ASME Trans. Mechatron.* **2018**, *23*, 875–882. [[CrossRef](#)]
17. Liu, X.; Hui, S.Y.R. Simulation Study and Experimental Verification of a Universal Contactless Battery Charging Platform with Localized Charging Features. *IEEE Trans. Power Electron.* **2007**, *22*, 2202–2210.
18. Hayt, W.H.; Buck, J.A. *Engineering Electromagnetics*, 8th ed.; The McGraw-Hill Companies, Inc.: New York, NY, USA, 2012; ISBN 978-0-07-338066-7.
19. Smythe, W.R. *Static and Dynamic Electricity*, 2nd ed.; McGraw-Hill: New York, NY, USA, 1988; pp. 270–271.
20. Simpson, J.; Lane, J.; Immer, C.; Youngquist, R. Simple Analytic Expressions for the Magnetic Field of a Circular Current Loop. NASA Technical Reports Server. Available online: <https://ntrs.nasa.gov/archive/nasa/casi.ntrs.nasa.gov/20010038494.pdf> (accessed on 17 October 2019).



© 2019 by the authors. Licensee MDPI, Basel, Switzerland. This article is an open access article distributed under the terms and conditions of the Creative Commons Attribution (CC BY) license (<http://creativecommons.org/licenses/by/4.0/>).